chemosensors

MDPI

Article

Detection of Polynitro Compounds at Low Concentrations by SERS Using Ni@Au Nanotubes

Alena Shumskaya [1], Elizaveta Kozhina [2], Sergey Bedin [2,3], Stepan Andreev [3], Ekaterina Kulesh [4], Alexander Rogachev [1,4], Maxim Yarmolenko [4], Ilya Korolkov [5,6], Artem Kozlovskiy [5,6], Maksim Zdorovets [5,6,7], Viktor Belyaev [8], Valeriya Rodionova [8] and Larissa Panina [8,9,*]

1 Institute of Chemistry of New Materials, National Academy of Sciences of Belarus, 220141 Minsk, Belarus; lunka7@mail.ru (A.S.); rogachev78@mail.ru (A.R.)
2 The Lebedev Physical Institute of the Russian Academy of Sciences, Moscow 119991, Russia; liza.kozhina.99@mail.ru (E.K.); sa.bedin@mpgu.su (S.B.)
3 Laboratory of Advanced Materials Physics, Moscow Pedagogical State University, Moscow 119435, Russia; andreev_stepan@mail.ru
4 Faculty of Physics and Information Technologies, Francisk Skorina Gomel State University, 246019 Gomel, Belarus; katrinamillers29@mail.ru (E.K.); simmak79@mail.ru (M.Y.)
5 Engineering Profile Laboratory, L.N. Gumilyov Eurasian National University, Nur-Sultan 010000, Kazakhstan; i.korolkov@inp.kz (I.K.); kozlovskiy.a@inp.kz (A.K.); mzdorovets@inp.kz (M.Z.)
6 The Institute of Nuclear Physics, Almaty 010000, Kazakhstan
7 Department of Intelligent Information Technologies, Ural Federal University, Ekaterinburg 620075, Russia
8 Institute of Physics, Mathematics and IT, Immanuel Kant Baltic Federal University, Kaliningrad 236041, Russia; vbelyaev@kantiana.ru (V.B.); vvrodionova@kantiana.ru (V.R.)
9 Department of Technology of Electronic Materials, National University of Science and Technology (MISIS), Moscow 119049, Russia
* Correspondence: lpanina@misis.ru

check for updates

Citation: Shumskaya, A.; Kozhina, E.; Bedin, S.; Andreev, S.; Kulesh, E.; Rogachev, A.; Yarmolenko, M.; Korolkov, I.; Kozlovskiy, A.; Zdorovets, M.; et al. Detection of Polynitro Compounds at Low Concentrations by SERS Using Ni@Au Nanotubes. *Chemosensors* **2022**, *10*, 306. https://doi.org/10.3390/chemosensors10080306

Academic Editor: Barbara Palys

Received: 29 June 2022
Accepted: 28 July 2022
Published: 2 August 2022

Abstract: The identification of high-energy compounds in trace concentrations not only in the laboratory, but also in field conditions is of particular interest. The process should be clear, easy, and well-recognizable. We formed SERS-active substrates by using elongated nickel nanotubes synthesized by electrochemical deposition in the pores of ion-track membranes and coated them with gold for further application in the detection of low concentrations of analytes. The substrates were characterized using various techniques to determine the morphology of the nanotubes and modifying gold layer. The possibility of obtaining two types of gold-layer morphology was shown: in the form of a smooth film up to 20–50 nm thick and a coating with nanoneedles up to 250 nm long. The electric fields around the nanotubes were simulated at a laser wavelength of 532 nm to demonstrate the influence of the gold-layer morphology on the field distribution. The "needle" morphology was chosen to form the most effective SERS-active substrates for detection of low concentrations of aromatic polynitro compounds. The spectral peaks were identified by comparing the model and experimental Raman spectra at concentrations down to 10^{-5} M. Within this limit, all peaks ("fingerprints" of the substance) were clearly distinguishable.

Keywords: template synthesis; magnetic nanotubes; Ni@Au nanocomposite; surface-enhanced Raman scattering (SERS); track-etched membranes; local E-field modelling

1. Introduction

Detection and identification of high-energy compounds are highly needed for preventing potential threats. In particular, so-called improvised explosive devices are of great concern since they can be made from a wide range of commercially available chemicals. These chemicals can be detected by several spectroscopic methods. One of the most highly selective and sensitive methods is mass spectrometry, but the implementation of real-time

measurements is difficult in out-of-laboratory conditions due to the requirements of complex sample preparation [1]. Fourier transform infrared (FTIR) and Raman spectroscopic techniques can be used with minimal sample preparation and are suitable for the identification of a wide range of explosives and related materials [2–4]. Using these methods, it is possible to detect the presence of explosives in solid, liquid, or gas forms within few minutes or even seconds. They also have a high selectivity due to a specific spectral response from each chemical compound, known as the IR or Raman fingerprint. However, a special interest is directed to the identification of such compounds not in laboratory, but in "field" conditions, which is practically impossible due to the low intensity of the Raman signal.

Surface Enhanced Raman Scattering (SERS) is particularly useful in the detection and identification of extremely small quantities of explosives [5]. Nanostructured substrates are needed to achieve Raman signal enhancement, which depends on the electric and chemical interactions between analytes and substrate. With the advances in nanotechnology, various SERS substrates have been used for trace-level detection [6–8]. In many cases, assemblies of nanoparticles of various shapes are used. In another approach, nanopatterned surfaces have been proposed as a more efficient SERS platform. Due to the development of synthesis techniques, the morphology of such surfaces and their composition can be varied, which makes it possible to optimize the substrates for specific applications. By varying the geometric parameters of nanostructures, it is possible to optimize the operating range of the substrate wavelength and use different sources of stimulating radiation [9]. This is important for shifting the operating mode to the wavelength region, where the substance under study has a weak luminescence, which prevents the recording of the SERS signal. The main mechanism of SERS signal amplification is electromagnetic, which is determined by the concentration of the electric field both at the sharp edges of the nanostructures and in the gaps between them [10]. Thus, by varying the shape of the nanostructures, it is possible to create optimal conditions for the localization of analyte molecules in the "hot spot" areas.

The synthesis of hybrid nanostructures instead of pure nanostructures for SERS also has led to higher gains due to the presence of "hot-spots" located at the interface between metals and metal-semiconductor substrates. These hybrid systems can significantly improve the reproducibility, sensitivity, and reliability of the SERS signal for high-performance sensors of various chemical/biological molecules [11,12]. Hybrid nanostructures can be obtained on a substrate by electromigration [13], electron-beam lithography, electrochemical metal growth, etc.

Substrates produced by electron-beam lithography are most effective for obtaining a system of ordered nanostructures [14]. The ordered nanostructures ensure the guaranteed enhancement of the SERS signal of the substance under study at different points of the SERS substrate. However, when switching to the mapping technique, when recording more than a hundred SERS spectra in the automatic mode, the probability of detecting a high intensity SERS spectrum of a molecule, located in the most favorable region relative to hot-spots, is high even on substrates with disordered nanostructures [15].

In another approach, core-shell hybrid nanostructures have been proposed as SERS substrates. Some examples include structures based on Ag-SiO_2, Au-SiO_2 [16], and Fe_3O_4/Au, which are usually obtained by wet-chemistry methods [17]. Carbon based hybrid nanostructures are also used for SERS, such as carbon nanotubes-Ag, carbon nanotubes-Au, graphene-plasmon metal, and graphene oxide-plasmon metal. These nanostructures can be obtained by thermal evaporation [18], magnetron sputtering [19], electrochemical deposition [20], and chemical vapor deposition.

A number of studies have demonstrated the ability of SERS-based methods for multiplex detection with high sensitivity [21,22]. An original method for the double detection of cancer biomarkers for rapid screening and biomolecular profiling has previously been proposed. The effectiveness of the method was demonstrated for three biomarkers, both individually and in combination. For further development of this method, it was suggested to employ a larger panel of antibodies and SERS nanotags. However, the main advantage

of the proposed method of determining low concentrations of biomarkers could be negated by the screening effect [23].

Nevertheless, a hybrid of micro and nanostructure consisting of a laser-textured stainless steel surface with spacing of 50 μm and coated with a 60 nm thick gold layer has previously been proposed for SERS detection at the femtomolar level [24]. Micro-nanostructured substrates can be efficiently produced based on polymer templates with a system of identical pore channels 30–400 nm in diameter and 3–10 microns in length using template synthesis methods, which can be filled with different metals. Owing to the template structure, they also can be used as highly efficient substrates [25]. However, a greater repeatability of a high-intensity signal is higher for metallic nanostructures grown in the template pores. Based on such polymer templates, nanostructures of various shapes can be obtained from pure metals: nanocones [26], nanowires [27], or nanotubes [28]. Recently, thanks to the development of synthesis methods, it has become possible to mass-scale the synthesis of nanostructures from several metals by layer-by-layer deposition [29] or by coating the resulting nanostructures with a layer of another metal [30].

Magnetic-plasmonic nanoparticles (NPs) made of a magnetic core coated with plasmonic metals are of particular interest for forming SERS substrates, as they offer advantages over nanostructures made of pure noble metals [31]. Firstly, magnetic-plasmonic NPs can be ordered by a magnetic field to form controlled hot-spots for optimal amplification of the Raman signal by several orders of magnitude [32,33], and to obtain a finer spectrum structure. Such SERS substrates may be used in medicine; for example, magneto-plasmonic nanotubes were proposed for the extremely sensitive and specific detection of trace BPA down to 100 ng mL^{-1} [34]. Secondly, the magnetic properties of NPs ensure the efficient extraction and separation from target substances. The possible control by an external magnetic field also simplifies many processes such as stirring. In addition, magneto-plasmonic NPs can be reused to decrease the cost of SERS investigations of analytes for users.

The development of cost-effective methods for fabricating stable magnetoplasmonic nanostructures that are industrially scalable, easily controllable, and reusable remains an important challenge in the nano-industry. In such systems, iron oxide nanoparticles are most actively used as a magnetic core [35,36], but the use of 3d metals with stronger ferromagnetic properties can be more advantageous. In this respect, bimetal nanostructures produced by template synthesis are of interest due to their well-established and repeatable fabrication technology and large surface area. Nanotubes (NTs) and nanowires (NWs) with a magnetic core/plasmon metal shell structure can satisfy many important requirements for SERS substrates including a high enhancement factor, good reproducibility, and easy preparation [37]. It is interesting to note that magnetic NTs and NWs coated with a thin biocompatible material, such as gold, could be potentially used to develop a new kind of therapy based on magneto-mechanical effect. The magnetic shape anisotropy greatly enhances the efficiency of magneto-mechanical actuation. In combination with alternating or rotating external magnetic fields this treatment could achieve high level of cell viability reduction at small concentrations of NTs/NWs.

When analyzing complex molecules at low concentrations it can be difficult to interpret the spectra for substances similar in nature. As a result of such processes as inhomogeneous broadening of an ensemble of molecules, the Stark effect, etc., the peaks in the spectrum can be broadened, which makes it difficult to compare the obtained experimental data with existing databases. On the other hand, high sensitivity and extreme levels of details are important for real-time detection and are required for safety. This can be provided either by the presence of stable hot-spots on the surface of the substrates, or by a high degree of concentration of analyte molecules around the hot-spots.

In this work, special attention is paid to the identification of high-energy compounds belonging to the group of trinitrobenzene compounds with the help of SERS using Ni@Au NTs as amplifying agents. For other types of spectroscopy, it would be difficult to make a selective detection of these compounds. We aim to compare the SERS detection of explosives and similarly structured materials using partial SERS spectra in order to accurately detect

substances of similar composition at low concentrations. Therefore, in this work, greater emphasis is placed on the morphology and optical properties of the gold coating.

The experimental results are compared with the Raman spectra modeling of the studied substances in the ORCA 5 package. The mathematical modeling of electric fields scattered by magneto-plasmonic NTs provides a basis for revealing the optimal morphology of gold plating for the identification of SERS spectra. This is important to prevent overestimation of the SERS enhancement factor when a two-dimensional simulation is used ignoring the electrostatic shielding caused by closely spaced plasmonic nanoparticles. In [23], 3D calculations of the amplification of local electric fields by silver nanoparticles distributed on dielectric spheres were performed for various concentrations of Ag nanoparticles. For densely situated Ag nanoparticles, the effect of shielding the incident radiation by the upper hemisphere was strong. Therefore, the probe molecules must be properly situated considering the SERS substrate topology.

2. Materials and Methods

Ni@Au NTs were fabricated by the use of a two-stage process: (i) nickel NTs were synthesized in the pores of ion-track matrices by the template-synthesis method at a voltage of 1.75 V in a two-electrode electrochemical cell using an aqueous solution of $NiSO_4 \times 6H_2O$ (100 g/L), H_3BO_3 (45 g/L) at room temperature, and (ii) gold was deposited on the NTs surface by the electroless wet-chemistry method from an aqueous solution of gold chloride with two concentrations of 0.005 M and 0.01 M and 1%-hydrofluoric acid at 25 °C for 30 s [35–37]. Track-etched membranes 12 μm thick with a pore diameter of 360 ± 20 nm and a density of 4×10^7 cm^{-2} were made of polyethylene terephthalate (PET) and used as templates. The length of the tubes was 10.2 ± 0.2 μm, which is less than the thickness of the PET template, to prevent the formation of nanotube overlaps. The NTs external diameters corresponded to the pore diameters. The internal diameters were 195 ± 20 nm, and the wall thickness was equal to 85 ± 10 nm [38].

The characteristics of the modified NTs were comprehensively studied. Structural features were examined using scanning electron microscopy (SEM, Hitachi TM3030, Tokyo, Japan), scanning transmission electron microscopy (STEM, Hitachi SU9000) at simultaneous bright-field and annular dark-field imaging regimes, transmission electron microscopy (TEM, JEOL JEM-100, Tokyo, Japan), and energy-dispersive X-ray analysis (EDA, JED-2300 Analysis Station at JEOL JCM-6000 Plus Neoscope microscope). The results of XRD analysis and magnetic parameters for similar systems were reported in [38].

For this, substrates containing magnetic Ni@Au NTs were prepared using an ultrasonic bath. Then, their conglomeration with alignment along magnetic lines was dried. Using an optical microscope at a magnification of 100×, micrographs of these reinforcing substrates were obtained. Solutions of analyte were deposited dropwise using a dispenser, no more than 5 μL, onto areas containing single nanotubes. Solutions of 10^{-2}–10^{-5} M in acetone were prepared for analysis. After that, the substrates with the analyte were dried in air. SERS spectra of $(NO_2)_3C_6H_2N(NO_2)CH_3$ and $C_6H_3N_3O_8$ molecules with concentrations from 10^{-2} to 10^{-5} M in acetone solution adsorbed at the layered array of magnetic-plasmonic Ni@Au NTs were recorded using a Senterra Raman microscope (Bruker) with a laser wavelength of 532 nm. The spectra were measured in the range from 600 to 1900 cm^{-1}. A laser radiation with a power of 2 mW was applied. During the measurements, the signal acquisition time was 2 s, and the final signal intensity was calculated as the average of 5 signal measurements at different points of the sample. The processing and construction of the spectra were carried out using the OPUS program.

An important issue surrounding nanostructured materials for SERS applications is the morphologic stability during laser-beam illumination. The minimum available exposition time and power settings were chosen for spectrum acquisition. Changes in the spectra during the study (decreasing in intensity by the end of the spectrum measurement) were not detected.

The geometric optimization of molecules and the determination of the wave numbers of Raman scattering and the activity of the tested substances were carried out using the ORCA 5.0.3 software package [39]. The numerical error of the frequency shift can reach 50 cm^{-1}, but in most cases it should be much smaller. This error can occur for several reasons, including various optimizations of molecular vibrations, or the use of simplifying assumptions such as replacing a molecular medium with a certain permittivity with a vacuum. However, the general form of the spectrum remains unchanged.

To study the electric field distribution and a possible SERS enhancement factor, the simulation was performed using the KARAT electromagnetic code with a monochromatic incident laser wavelength of 532 nm [40].

3. Results and Discussion

The surface morphology and elemental content of the fabricated structures are presented in Figure 1. The nickel NTs had a polycrystalline structure [34], and their surface had a pronounced granular morphology with level changes (bumps) of at least 5 nm, due to irregularities on the walls of the polymer pores formed during etching, as well as due to processing. The SEM images demonstrate that the morphology of the nickel NTs with gold coating depended on the concentration of gold ions in the solutions used for Au deposition. At a concentration of 0.005 M, the gold coating formed a thin film about 20–50 nm thick with fragments of gold particles 50–70 nm in size (Figure 1e). At a higher concentration of 0.01 M, gold nanostructures grew on the surface in the form of needles up to 150–250 nm long, which evenly covered the surface (Figure 1h). The content of elements corresponded to 100% of Ni for the bare Ni NTs, 78.3% of Ni and 21.7% of Au for the NTs coated with a layer of Au (0.005 M) and 48.3% of Ni and 51.7% of Au for the NTs coated with Au needles (0.01 M).

Modelling of the electric field around each of the obtained types of nanotubes (and also around the pure gold nanotubes) was carried out in order to determine the most efficient parameters for their use as SERS enhancement substrates.

The simulation was performed for the case of the pure nickel and "ideal" gold nanotubes (i.e., without roughness) with a wall thickness of 80 nm and a diameter of 400 nm. This was compared to core/shell NTs; a nickel tube core with a wall thickness of 100 nm, covered with a gold shell 20 nm thick. Finally, the structure of the nickel NTs coated with gold needles 150 nm long and 20 nm thick was also studied. The excitation by a laser pulse propagating perpendicular to the NTs axis (y-axis) along the x-direction was considered. The light was linearly polarized with a transverse electric field E_{0z}. The normalized electric field amplitude E/E_0 was obtained by the following procedure: the field amplitudes were calculated at all points of the computational domain (x-z plane) at each moment of time, and then the ratio of the field amplitude at a certain point to the incident wave amplitude E_0 was determined.

A large E-field was found to be on the edges of the nanotubes, at a gold shell/environment interface (Figure 2a,c,d). Figure 2b confirms that pure nickel nanotubes did not cause E-field localization. The highest E-field enhancement was observed using the NTs covered by an ensemble of golden needles (Figure 2d). This electric field localization is known as tip "hot-spots". The modelling results decisively demonstrated that the coating metal and morphology were very important for the subsequent use of such nanotubes as SERS active surfaces.

The effects of shielding the field inside the nanotube when laser radiation was applied to its side surface is also worth mentioning. As can be seen from Figure 2a,b, the shielding effect depended on the nanotube material. When pure gold nanotubes were used, the shielding was much less than when nickel was used. In the resulting SERS spectrum, there will be practically no contribution from the analyte molecules adsorbed inside the nanotube.

As shown in [41], the SERS signal gain (enhancement factor, EF) is proportional to the field enhancement as $(E/E_0)^4$, considering its average over all illuminated molecules. The maximum E/E_0 value for NTs coated with gold needles was estimated at 28.3 at

sharp edges (Figure 2d). A similar field enhancement for dendritic nanostructures was demonstrated in [42,43]. The maximum value of E/E_0 for NTs made of pure gold and nickel with a smooth surface was 2.8 and 2.2, respectively (Figure 2a,b). The field enhancement caused by Ni NTs was weaker compared to Au NTs and the latter had a much wider gain zone. For Ni NTs coated with a smooth gold layer, the maximum E/E_0 value was 2.33 (Figure 2c). Therefore, Au NTs received the greatest field enhancement, but their production is complicated. The combination of Ni NTs and a thin layer of gold, which is easier to synthesize, could be promising for achieving a strong field enhancement but a more complex gold-layer morphology is required.

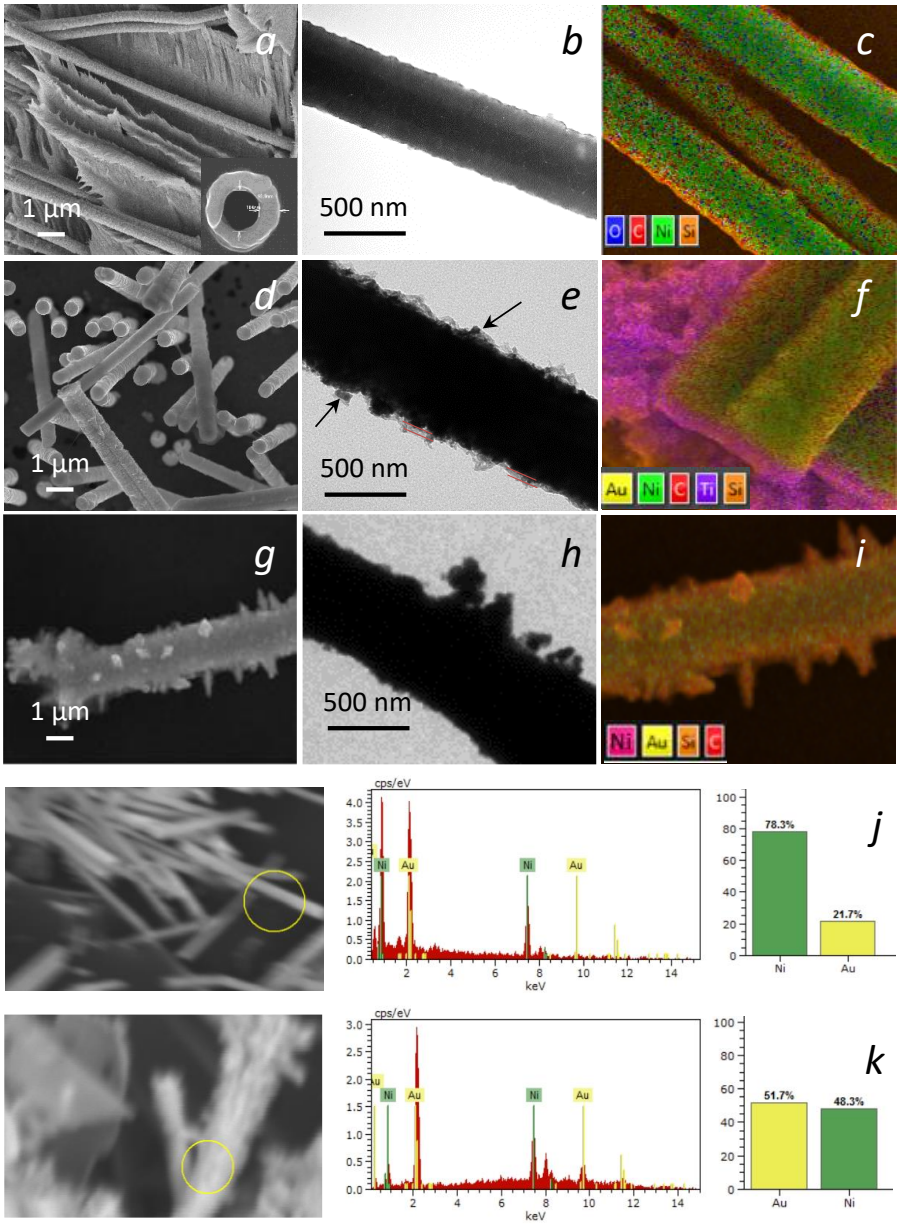

Figure 1. Images and elemental content mapping of fabricated structures. Nickel NTs: SEM (**a**), TEM (**b**) and EDX-mapping (**c**). Ni@Au with thin gold layer: SEM (**d**), TEM (**e**), EDX-mapping (**f**), and elemental composition (**j**). Ni@Au with gold needles: SEM (**g**), TEM (**h**), EDX-mapping (**i**), and elemental composition (**k**).

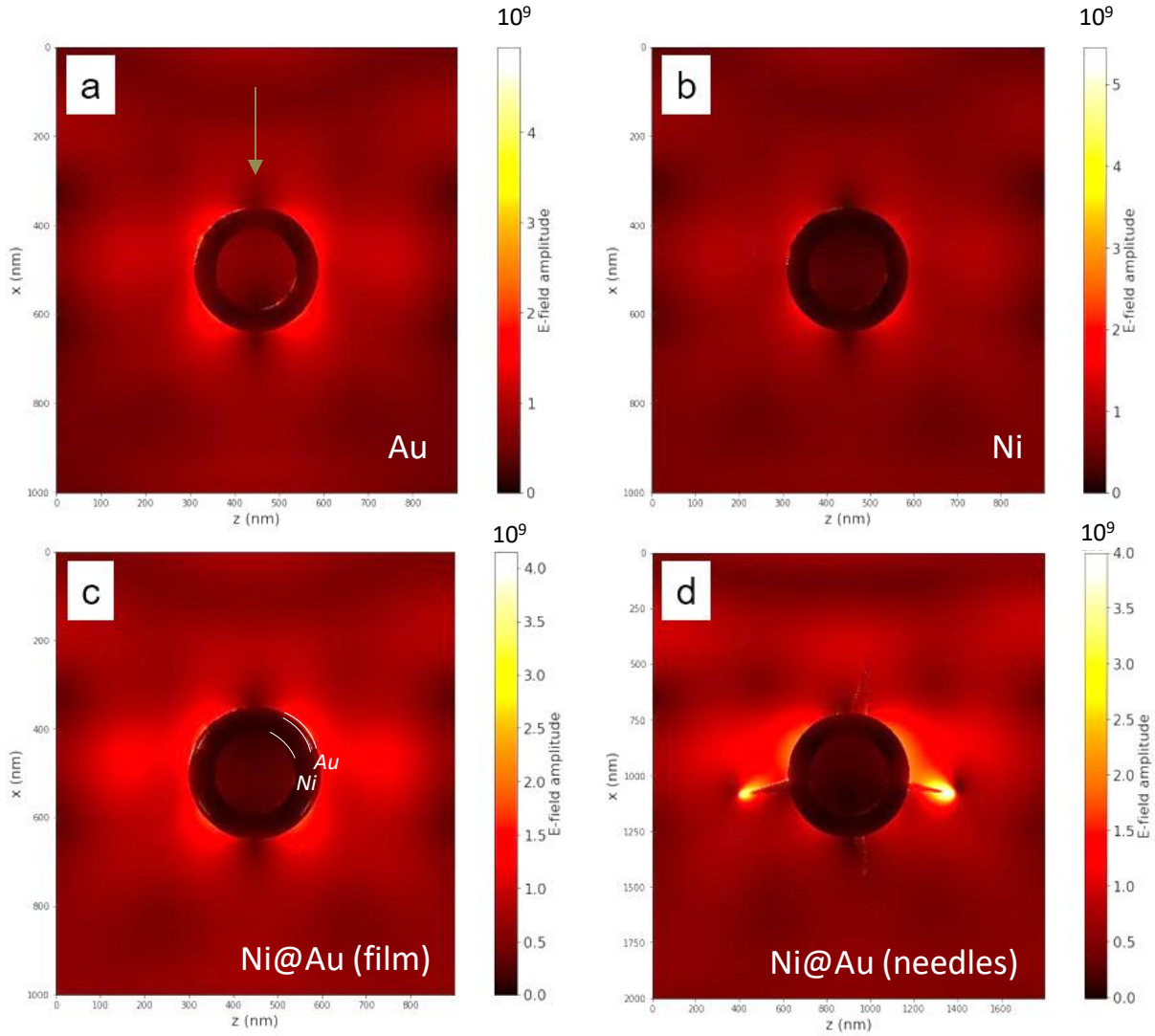

Figure 2. Electric field distribution around Ni/Au nanostructures. (**a**) Nanotubes made of pure gold, (**b**) nanotubes made of pure nickel, (**c**) core/shell (nickel/gold) nanotubes with a smooth Au layer, (**d**) Ni nanotubes covered by a uniform layer of Au needles. The exiting radiation wavelength was 532 nm.

This was realized in Ni@Au NTs with a needle-type morphology of Au coating. The field enhancement at the sharp edges of the needles was about 12.14 which theoretically can provide a SERS enhancement factor of more than 2×10^4. This result was consistent with previous studies [36] where the highest SERS gain was obtained for NTs with a developed spike-like Au morphology. Therefore, based on the modelling results, this type of Ni@Au NTs was selected to form SERS substrates.

The idea of rapid detection of substances in the field is based on several factors:

i. Simple and efficient sample preparation and preparation of equipment for operation.
ii. A simple and fast detection technique with a portable device, and there should be no need to create special conditions for measurements.
iii. A reliable signal processing technique allowing the obtaining of a full spectrum from a partial spectrum. The option of comparison with the library of substance spectra or with calculated spectra should be provided.

In this work, we tried to partially satisfy these requirements by synthesizing Ni@Au nanotubes and preparing a suspension based on them, proposing various methods for the

formation of active substrates, and reconstructing the theoretical spectra of the analyzed substances, followed by their comparison with those obtained experimentally.

In order to determine the effectiveness of detecting low concentrations using substances with Ni@Au NTs, the following aromatic nitro-compounds with various functional groups were selected: $(NO_2)_3C_6H_2N(NO_2)CH_3$ and $C_6H_3N_3O_8$. The SERS analysis of the aromatic nitrates was carried out for concentrations of 10^{-2}–10^{-5} mol/L.

There are two basic options for sample preparations and the formation of SERS active substrates using hybrid nanotubes and for the experimental analysis of substances [31,36,44]:

1. Add a suspension of functionalized nanotubes at a concentration of 1 mg/mL to the analyte solution. Then, the NTs need to be concentrated in a solution with a magnet and deposited on a single-crystal silicon substrate. The NTs are spread evenly over the surface with a magnet and dried.
2. Preliminarily apply functionalized nanotubes from the suspension onto a single-crystal silicon plate, distribute them with a magnet, and dry. Apply the analyte solution.

Both methods were tested by us earlier [37,44] and it was found that method 2 is easier to operate and gives better results, which is probably due to a more uniform distribution of nanotubes over the surface during the preliminary preparation of the SERS active substrate. The first method was proposed in [37] using a standard dye Methylene Blue ($C_{16}H_{18}ClN_3S$) at concentrations of 10^{-4}–10^{-6} M. The average value of EF of the SERS signal was about 10^4. The second method was used in [44]. In this work, Radomin 6G (R6G) molecules with concentrations of 10^{-3}–10^{-8} M adsorbed on an array of Ni@Au nanotubes were recorded. The average EF was estimated as 8×10^5. In addition, it was shown that the enhancement of the SERS signal is greater on single NTs than on their conglomerates, which requires careful distribution of functionalized nanotubes over the surface. The alignment can be achieved using template-assisted electrodeposition techniques [45], which is potentially possible with the considered structures.

Microphotographs of the Ni@Au NTs surface with adsorbed analyte substances $(NO_{2)3}C_6H_2N(NO_2)CH_3$ of different concentrations are shown in Figure 3. The analyte droplet was contracted and therefore its molecules were concentrated around the nanotubes, which is favorable to further increase the intensity of the SERS signal. This contraction effect, well-known as a coffee-ring effect [46], is observed when a drop of analyte is applied to glass or foil with a pinned contact line. However, in the case of nanotubes, the concentration occured precisely around them, and not at the edges of the drop. It is assumed that this was due to the surface charge of the nanotubes (+), while the contraction of the droplet on the glass is mainly due to the effect of surface tension. The contraction of the analyte droplet to the plasmonic nanostructures increased the intensity of the SERS signal due to the chemical effect of molecule concentration.

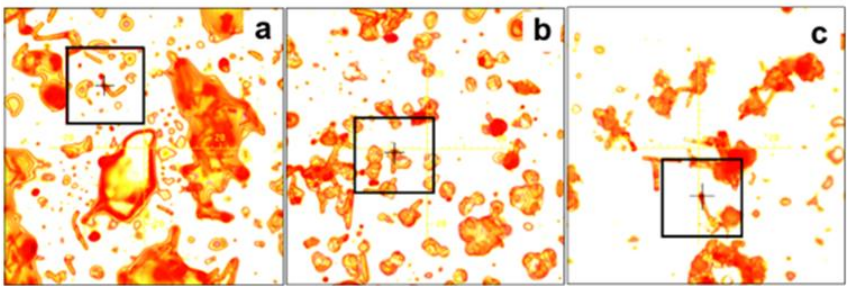

Figure 3. Micrographs of samples of the SERS-active substrate of Au@Ni nanotubes with analytes $(NO_{2)3}C_6H_2N(NO_2)CH_3$ at various concentrations: (**a**) -10^{-2} M, (**b**) -10^{-3} M, (**c**) -10^{-4} M. The analyzed area is marked with a square, the area under study is of 20×20 μm^2. The laser beam is concentrated in the center of the square.

The SERS spectra for different concentrations of the adsorbed analyte substances using Ni@Au NTs, are shown in Figure 4a,b. The calculated spectra are given in Figure 4c,d.

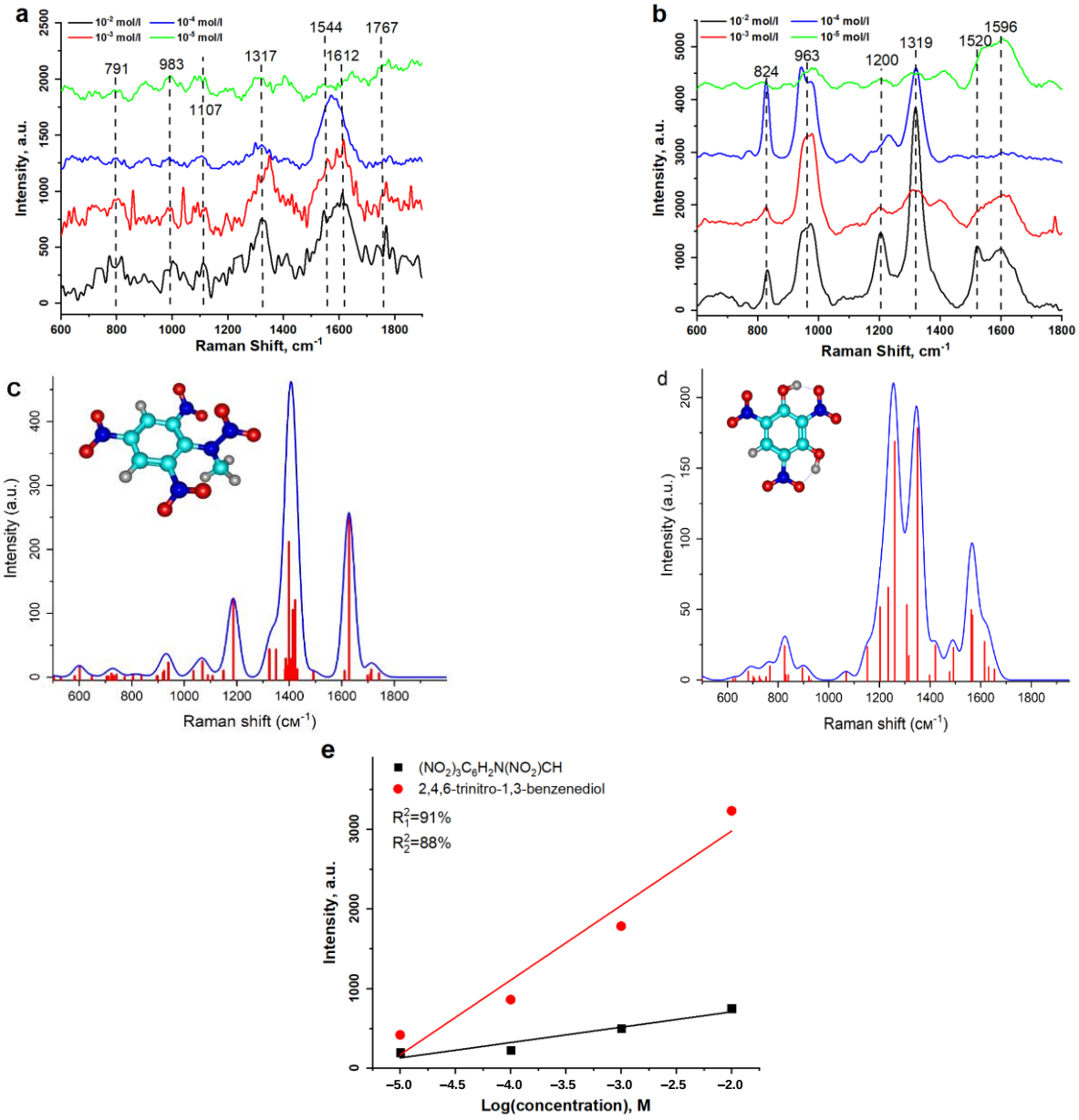

Figure 4. Measured and calculated SERS spectra. (**a**)—measured SERS spectra for $(NO_2)_3C_6H_2N(NO_2)CH_3$ at concentrations of 10^{-2}–10^{-5} M, (**b**)—measured SERS spectra for 2,4,6-trinitro-1,3-benzenediol at concentrations of 10^{-2}–10^{-5} M. (**c**,**d**)—theoretical Raman spectra for $(NO_2)_3C_6H_2N(NO_2)CH_3$ and 2,4,6-trinitro-1,3-benzenediol, respectively. (**e**)—calibration curves where the averaged peak intensities of the 1317 cm^{-1} band was plotted as a function of the logarithmic concentration of $(NO_2)3C_6H_2N(NO_2)CH_3$ and the same for the peak intensities of the 1319 cm^{-1} band of 2,4,6-trinitro-1,3-benzenediol.

For each concentration of both analytes, the SERS spectra were taken from several randomly selected spots on the substrate surface (on the surface of single NTs) and subsequently averaged. For $(NO_2)_3C_6H_2N(NO_2)CH_3$, the experimental spectrum was dominated by peaks around 1600 cm^{-1}, which were responsible for C=C aromatic stretching vibration due to the large Raman cross-section of the aromatic ring. The spectrum was also characterized by the presence of a peak in the range 1317–1335 cm^{-1}, which was responsible for the symmetric stretching vibration of the NO_2 group and is one of the distinctive peaks for this substance. It should be noted that the presence of this peak was also preserved for such a low concentration as 10^{-5} M. The experimental spectra showed a peak at 1767 cm^{-1},

which is also characteristic of the nitro group. The general form of the spectrum curve fully corresponded to theoretical calculations (Figure 4c).

The SERS spectrum of the $C_6H_3N_3O_8$ molecule is shown in Figure 4b. The spectra obtained for different concentrations of the substance were dominated by peaks at 1319 cm^{-1}, which correspond to the symmetric stretching vibration of the NO_2 group. The shape of the spectral curve, as well as the positions of the peaks, were in complete agreement with the calculated spectrum (Figure 4d), except for the peak at 963 cm^{-1}, which is characteristic of silicon vibrations (the surface on which the nanotubes were deposited).

To determine the difference in the spectra of the two different substances related to aromatic polynitroamines, it is enough to pay attention to the region 1200–1400 cm^{-1}, which is characteristic of vibrations of the NO_2 group. Precise identification of $(NO_2)_3C_6H_2N(NO_2)CH_3$ and $C_6H_3N_3O_8$ was possible by the number of characteristic peaks (one or two, respectively) for concentrations down to 10^{-4} M, but somewhat more difficult for 10^{-5} M due to inhomogeneous broadening and a weak concentration effect. It is also worth noting the presence of a characteristic peak at 1767 cm^{-1}, which is also typical of the nitro group for $(NO_2)_3C_6H_2N(NO_2)CH_3$. For $C_6H_3N_3O_8$, this peak was absent both in the experimental and theoretical spectra, which makes it possible to clearly understand which polynitroamine was registered.

For the calculated Raman spectrum of $(NO_2)_3C_6H_2N(NO_2)CH_3$, the peaks at 1187, 1431, 1491, 1611, 1628 cm^{-1} were responsible for benzene ring, the 1069 cm^{-1} peak was for fluctuations of CH_3 group and the peaks at 1698, 1709, 1712 cm^{-1} were for fluctuations of NO_2 group. While for the calculated Raman spectrum of $C_6H_3N_3O_8$ the peaks at 825, 1349, 1615, 1630 and 1654 cm^{-1} were responsible for NO_2. The peaks at 1152, 1203 and 1260 cm^{-1} were responsible for C-N bonds. The peaks at 1308 and 1316 cm^{-1} were responsible for benzene ring, C-O, and C-N bonds. Hydrogen bonds appeared on the spectrum at 1421 and 1492 cm^{-1}. Benzene rings appeared on the spectrum at 1562 and 1567 cm^{-1}.

The calibration curves which present the averaged peak intensities of the 1317 cm^{-1} and 1319 cm^{-1} bands vs. the logarithmic concentrations of $(NO_2)_3C_6H_2N(NO_2)CH_3$ and 2,4,6-trinitro-1,3-benzenediol, respectively, are shown in Figure 4e. Using these data, the limit of detection (LOD) for the two substances was determined as $10^{-5.9}$ M and $10^{-6.4}$ M, respectively. Such an approach for LOD investigation is the most appropriate for substances with a high luminescence level. We consider such a limit of detection to be sufficient for fast (out-of-laboratory) substance identification.

It was reported that SERS substrates consisting of Ni nanowires made possible the identification of SudanII solution with a concentration of 10^{-5} M [47]. This was explained by tip enhanced Raman scattering. The level of detection is similar to that obtained with the use of Ni@Au NTs, however, in our case randomly oriented nanotubes were used. Ordered Ni@Au NTs will provide much higher EF and lower LOD [44].

Thus, the experimental spectra were well consistent with the calculated ones, which makes it possible to create a local database of the spectra of substances, to isolate these substances when working in a mixture of several substances, and to create software that compares the calculated and practical experience.

4. Conclusions

Ni@Au core-shell magnetoplasmonic nanotubes 10 ± 0.2 μm in length were synthesized by a two-stage method including nickel nanotube growth in pores of PET ion-track templates and electroless wet-chemical functionalizing with a gold layer in the form of a smooth coating or a coating with nanoneedles. Such functionalization did not bring changes to the magnetic core-nickel nanotubes, because neither the structural nor magnetic properties changed noticeably. The optical properties of the two distinct morphologies were investigated by simulation confirming a strong electric field enhancement at the needle edges. These NTs were used as substrates for the SERS method.

The possibility of accurate detection of aromatic polynitroamines (trinitroamines) with different functional groups using SERS with the developed substrates was demonstrated. It

was possible not only to accurately determine the type of substance, but specifically name it and distinguish it from a similar one in composition. The use of Ni@Au core-shell magnetic nanotubes made it possible to amplify the signal from aromatic polynitroamines due to the effect of plasmon resonance observed when the structures were irradiated with light. The possibility of using the synthesized Ni@Au core-shell magnetic nanotubes for SERS was demonstrated using $(NO_2)_3C_6H_2N(NO_2)CH_3$ and $C_6H_3N_3O_8$ analytes. The amplification of Raman signals for concentrations up to 10^{-5} M for $(NO_2)_3C_6H_2N(NO_2)CH_3$ and $C_6H_3N_3O_8$ was estimated. To demonstrate the significant accuracy of the reproduction of the spectra of substances using the SERS method, the Raman spectra of substances were simulated and, by comparing the characteristic peaks, the correspondence between the calculated and experimentally obtained spectra was shown. Ni@Au NTs are promising for use in chemo- and biosensorics by active SERS.

Author Contributions: Conceptualization, A.S. and L.P.; methodology, I.K. and A.R., fabrication, I.K.; software, E.K. (Elizaveta Kozhina), S.B. and S.A.; modelling, S.A.; validation, A.K., M.Z. and M.Y.; structural characterization A.K. and M.Z.; formal analysis, A.R., S.B., E.K. (Elizaveta Kozhina) and V.B.; investigation, M.Y.; writing—original draft preparation, A.S., E.K. (Elizaveta Kozhina), S.B. and E.K. (Ekaterina Kulesh); writing—review and editing, V.B., L.P. and V.R.; visualization, A.S. and E.K. (Elizaveta Kozhina); funding acquisition, L.P. and S.B. All authors have read and agreed to the published version of the manuscript.

Funding: Works on theoretical modeling were carried out within the framework of the State Contract of the Moscow Pedagogical State University (MPGU) "Physics of the perspective materials and nanostructures: basic researches and applications in material sciences, nanotechnologies and photonics" supported by the Ministry of Science and Higher Education of the Russian Federation (AAAA-A20-120061890084-9). S.B. and E.K. (Elizaveta Kozhina) are members of the scientific school SS-776.2022.1.2. Works on NTs fabrication and characterization were supported by the Russian Science Foundation, grant number 21-72-20158 (NTs as tool for magneto-mechanical treatment).

Informed Consent Statement: Not applicable.

Acknowledgments: The authors are grateful for help with SERS measurements to graduate students S. Lukkareva and D. Khairetdinova.

Conflicts of Interest: The authors declare no conflict of interest.

References

1. Barron, L.; Gilchrist, E. Ion chromatography-mass spectrometry: A review of recent technologies and applications in forensic and environmental explosives analysis. *Anal. Chim. Acta* **2014**, *806*, 27–54. [CrossRef] [PubMed]
2. López-López, M.; García-Ruiz, C. Infrared and Raman spectroscopy techniques applied to identification of explosives. *TrAC Trends Anal. Chem.* **2014**, *54*, 36–44. [CrossRef]
3. Ben-Jaber, S.; Peveler, W.J.; Quesada-Cabrera, R.; Sol, C.W.O.; Papakonstantinou, I.; Parkin, I.P. Sensitive and specific detection of explosives in solution and vapour by surface-enhanced Raman spectroscopy on silver nanocubes. *Nanoscale* **2017**, *9*, 16459–16466. [CrossRef] [PubMed]
4. Doty, K.C.; Muro, C.K.; Bueno, J.; Halámková, L.; Lednev, I.K. What can Raman spectroscopy do for criminalistics? *J. Raman Spectrosc.* **2016**, *47*, 39–50. [CrossRef]
5. Milligan, K.; Shand, N.C.; Graham, D.; Faulds, K. Detection of Multiple Nitroaromatic Explosives via Formation of a Janowsky Complex and SERS. *Anal. Chem.* **2020**, *92*, 3253–3261. [CrossRef] [PubMed]
6. Wackerbarth, H.; Salb, C.; Gundrum, L.; Niederkruger, M.; Christou, K.; Beushausen, V.; Viol, W. Detection of explosives based on surface-enhanced Raman spectroscopy. *Appl. Opt.* **2010**, *49*, 4362–4366. [CrossRef]
7. Hakonen, A.; Wu, K.; Stenbaek Schmidt, M.; Andersson, P.O.; Boisen, A.; Rindzevicius, T. Detecting forensic substances using commercially available SERS substrates and handheld Raman spectrometers. *Talanta* **2018**, *189*, 649–652. [CrossRef] [PubMed]
8. Jamil, A.K.M.; Izake, E.L.; Sivanesan, A.; Fredericks, P.M. Rapid detection of TNT in aqueous media by selective label free surface enhanced Raman spectroscopy. *Talanta* **2015**, *134*, 732–738. [CrossRef] [PubMed]
9. Ding, W.; Bachelot, R.; Kostcheev, S.; Royer, P.; Espiau de Lamaestre, R. Surface plasmon resonances in silver Bowtie nanoantennas with varied bow angles. *J. Appl. Phys.* **2010**, *108*, 124314. [CrossRef]
10. Radziuk, D.; Moehwald, H. Prospects for plasmonic hot spots in single molecule SERS towards the chemical imaging of live cells. *Phys. Chem. Chem. Phys.* **2015**, *17*, 21072–21093. [CrossRef] [PubMed]
11. Barbillon, G. Fabrication and SERS Performances of Metal/Si and Metal/ZnO Nanosensors: A Review. *Coatings* **2019**, *9*, 86. [CrossRef]

12. Fateixa, S.; Nogueira, H.I.; Trindade, T. Hybrid nanostructures for SERS: Materials development and chemical detection. *Phys. Chem. Chem. Phys.* **2015**, *17*, 21046–21071. [CrossRef]
13. Ward, D.R.; Grady, N.K.; Levin, C.S.; Halas, N.J.; Wu, Y.; Nordlander, P.; Natelson, D. Electromigrated nanoscale gaps for surface-enhanced Raman spectroscopy. *Nano. Lett.* **2007**, *7*, 1396–1400. [CrossRef]
14. Cinel, N.A.; Cakmakyapan, S.; Butun, S.; Ertas, G.; Ozbay, E. E-Beam lithography designed substrates for surface enhanced Raman spectroscopy. *Photonics Nanostruct. Fundam. Appl.* **2015**, *15*, 109–115. [CrossRef]
15. Farcau, C.; Astilean, S. Mapping the SERS Efficiency and Hot-Spots Localization on Gold Film over Nanospheres Substrates. *J. Phys. Chem. C* **2010**, *114*, 11717–11722. [CrossRef]
16. Rodríguez-Fernández, D.; Langer, J.; Henriksen-Lacey, M.; Liz-Marzán, L.M. Hybrid Au–SiO_2 Core–Satellite Colloids as Switchable SERS Tags. *Chem. Mater.* **2015**, *27*, 2540–2545. [CrossRef]
17. Faure, A.C.; Barbillon, G.; Ou, M.; Ledoux, G.; Tillement, O.; Roux, S.; Fabregue, D.; Descamps, A.; Bijeon, J.L.; Marquette, C.A.; et al. Core/shell nanoparticles for multiple biological detection with enhanced sensitivity and kinetics. *Nanotechnology* **2008**, *19*, 485103. [CrossRef]
18. Jorio, A.; Pimenta, M.A.; Filho, A.G.S.; Saito, R.; Dresselhaus, G.; Dresselhaus, M.S. Characterizing carbon nanotube samples with resonance Raman scattering. *New J. Phys.* **2003**, *5*, 139. [CrossRef]
19. Gohil, S.; Ghosh, S. Surface enhanced Raman scattering from multiwalled carbon nanotubes at low temperatures. *Appl. Phys. Lett.* **2010**, *96*, 143108. [CrossRef]
20. Liu, Y.; Hu, Y.; Zhang, J. Few-Layer Graphene-Encapsulated Metal Nanoparticles for Surface-Enhanced Raman Spectroscopy. *J. Phys. Chem. C* **2014**, *118*, 8993–8998. [CrossRef]
21. Dey, S.; Trau, M.; Koo, K.M. Surface-Enhanced Raman Spectroscopy for Cancer Immunotherapy Applications: Opportunities, Challenges, and Current Progress in Nanomaterial Strategies. *Nanomaterials* **2020**, *10*, 1145. [CrossRef] [PubMed]
22. Dey, S.; Ahmed, E.; Somvanshi, P.S.; Sina, A.A.I.; Wuethrich, A.; Trau, M. An Electrochemical and Raman Scattering Dual Detection Biosensor for Rapid Screening and Biomolecular Profiling of Cancer Biomarkers. *Chemosensors* **2022**, *10*, 93. [CrossRef]
23. Wang, F.; Du, D.; Liu, S.; Wang, L.; Jiao, T.; Xu, Z.; Wang, H. Revealing the Hemispherical Shielding Effect of SiO_2@Ag Composite Nanospheres to Improve the Surface Enhanced Raman Scattering Performance. *Nanomaterials* **2021**, *11*, 2209. [CrossRef] [PubMed]
24. Yang, H.; Gun, X.; Pang, G.; Zheng, Z.; Li, C.; Yang, C.; Wang, M.; Xu, K. Femtosecond laser patterned superhydrophobic/hydrophobic SERS sensors for rapid positioning ultratrace detection. *Opt. Express* **2021**, *29*, 16904–16913. [CrossRef]
25. Kovalets, N.P.; Kozhina, E.P.; Razumovskaya, I.V.; Bedin, S.A.; Piryazev, A.A.; Grigoriev, Y.V.; Naumov, A.V. Toward single-molecule surface-enhanced Raman scattering with novel type of metasurfaces synthesized by crack-stretching of metallized track-etched membranes. *J. Chem. Phys.* **2022**, *156*, 034902. [CrossRef] [PubMed]
26. Skibinska, K.; Smola, G.; Bialo, L.; Kutyla, D.; Kolczyk-Siedlecka, K.; Kwiecinska, A.; Wojnicki, M.; Zabinski, P. Influence of Annealing Time of Aluminum AA1050 on the Quality of Cu and Co Nanocones. *J. Materi. Eng. Perform.* **2020**, *29*, 8025–8035. [CrossRef]
27. Bedin, S.A.; Rybalko, O.G.; Polyakov, N.B.; Zagorskii, D.L.; Razumovskaya, A.V.; Bondarenko, G.G.; Oleinikov, V.A. Metal micro- and nanowires fabricated by matrix synthesis and their application in mass spectrometry. *Inorg. Mater. Appl. Res.* **2010**, *1*, 359–364. [CrossRef]
28. Shumskaya, A.; Bundyukova, V.; Kozlovskiy, A.; Zdorovets, M.; Kadyrzhanov, K.; Kalkabay, G.; Kaniukov, E. Evolution of morphology, structure, and magnetic parameters of Ni nanotubes with growth in pores of a PET template. *J. Magn. Magn. Mater.* **2020**, *497*, 165913. [CrossRef]
29. Kozlovskiy, A.; Zdorovets, M.; Kadyrzhanov, K.; Korolkov, I.; Rusakov, V.; Nikolaevich, L.; Fesenko, O.; Budnyk, O.; Yakimchuk, D.; Shumskaya, A.; et al. FeCo nanotubes: Possible tool for targeted delivery of drugs and proteins. *Appl. Nanosci.* **2018**, *9*, 1091–1099. [CrossRef]
30. Roselina, N.R.; Azizan, A.; Hyie, K.M.; Murad, M.C.; Abdullah, A.H. Synthesis and characterization of Ni-Au bimetallic nanoparticles. *Int. J. Mod. Phys. B* **2015**, *29*, 1540006. [CrossRef]
31. Song, D.; Yang, R.; Long, F.; Zhu, A. Applications of magnetic nanoparticles in surface-enhanced Raman scattering (SERS) detection of environmental pollutants. *J. Environ. Sci. China* **2019**, *80*, 14–34. [CrossRef] [PubMed]
32. Kumar, G.V.P.; Rangarajan, N.; Sonia, B.; Deepika, P.; Rohman, N.; Narayana, C. Metal-coated magnetic nanoparticles for surface enhanced Raman scattering studies. *Bull. Mater. Sci.* **2011**, *34*, 207–216. [CrossRef]
33. Kozhina, E.; Kulesh, E.; Bedin, S.; Doludenko, I.; Piryazev, A.; Korolkov, I.; Kozlovskiy, A.; Zdorovets, M.; Rogachev, A.; Shumskaya, A. One-Dimensional Magneto-Optical Nanostructures: Template Synthesis, Structure, Properties, and Application in Spectroscopy Based on Plasmon Resonance. *IEEE Magn. Lett.* **2022**, *13*, 1–5. [CrossRef]
34. Sen, L.; He, D.; Li, S.; Chen, R.; Peng, Y.; Li, S.; Han, D.; Wang, Y.; Qin, K.; Ren, S.; et al. Magnetic Halloysite Nanotube-Based SERS Biosensor Enhanced with Au@Ag Core—Shell Nanotags for Bisphenol A Determination Enhanced Reader. *Biosensors* **2022**, *12*, 387–400.
35. Kazemi, M. Based on magnetic nanoparticles: Gold reusable nanomagnetic catalysts in organic synthesis. *Synth. Commun.* **2020**, *50*, 2079–2094. [CrossRef]
36. Shokouhimehr, M. Magnetically Separable and Sustainable Nanostructured Catalysts for Heterogeneous Reduction of Nitroaromatics. *Catalysts* **2015**, *5*, 534–560. [CrossRef]

37. Shumskaya, A.; Korolkov, I.; Rogachev, A.; Ignatovich, Z.; Kozlovskiy, A.; Zdorovets, M.; Anisovich, M.; Bashouti, M.; Shalabny, A.; Busool, R.; et al. Synthesis of Ni@Au core-shell magnetic nanotubes for bioapplication and SERS detection. *Colloids Surf. A Physicochem. Eng. Asp.* **2021**, *626*, 127077. [CrossRef]
38. Shumskaya, A.; Panina, L.; Rogachev, A.; Ihnatovich, Z.; Kozlovskiy, A.; Zdorovets, M.; Kaniukov, E.; Korolkov, I. Catalytic Activity of Ni Nanotubes Covered with Nanostructured Gold. *Processes* **2021**, *9*, 2279. [CrossRef]
39. Neese, F. Software update: The ORCA program system—Version 5.0. *WIREs Comput. Mol. Sci.* **2022**, *8*, e1327. [CrossRef]
40. Tarakanov, V.P. Code KARAT in simulations of power microwave sources including Cherenkov plasma devices, vircators, orotron, E-field sensor, calorimeter etc. *EPJ Web Conf.* **2017**, *149*, 04024. [CrossRef]
41. Langer, J.; Jimenez de Aberasturi, D.; Aizpurua, J.; Alvarez-Puebla, R.A.; Auguie, B.; Baumberg, J.J.; Bazan, G.C.; Bell, S.E.J.; Boisen, A.; Brolo, A.G.; et al. Present and Future of Surface-Enhanced Raman Scattering. *ACS Nano* **2020**, *14*, 28–117. [CrossRef]
42. Kozhina, E.P.; Andreev, S.N.; Tarakanov, V.P.; Bedin, S.A.; Doludenko, I.M.; Naumov, A.V. Study of Local Fields of Dendrite Nanostructures in Hot Spots Formed on SERS-Active Substrates Produced via Template-Assisted Synthesis. *Bull. Russ. Acad. Sci. Phys.* **2021**, *84*, 1465–1468. [CrossRef]
43. Yakimchuk, D.V.; Kaniukov, E.Y.; Lepeshov, S.; Bundyukova, V.D.; Demyanov, S.E.; Arzumanyanm, G.M.; Doroshkevich, N.V.; Mamatkulov, K.Z.; Bochmann, A.; Presselt, M.; et al. Self-organized spatially separated silver 3D dendrites as efficient plasmonic nanostructures for surface-enhanced Raman spectroscopy applications. *J. Appl. Phys.* **2019**, *126*, 233105. [CrossRef]
44. Korolkov, I.V.; Shumskaya, A.; Kozlovskiy, A.L.; Kaliyekperov, M.E.; Lissovskaya, L.I.; Zdorovets, M.V. Magnetic-plasmonic Ni nanotubes covered with gold for improvement of SERS analysis. *J. Alloy. Compd.* **2022**, *901*, 163661. [CrossRef]
45. Zhu, C.; Meng, G.; Zheng, P.; Huang, Q.; Li, Z.; Hu, X.; Wang, X.; Huang, Z.; Li, F.; Wu, N. A Hierarchically Ordered Array of Silver-Nanorod Bundles for Surface-Enhanced Raman Scattering Detection of Phenolic Pollutants. *Adv. Mater* **2016**, *28*, 4871–4876. [CrossRef]
46. Deegan, R.D.; Bakajin, O.; Dupont, T.F.; Huber, G.; Nagel, S.R.; Witten, T.A. Capillary flow as the cause of ring stains from dried liquid drops. *Nature* **1997**, *389*, 827–829. [CrossRef]
47. Zhang, L.; Fang, Y.; Zhang, P. Laser-MBE of nickel nanowires using AAO template: A new active substrate of surface enhanced Raman scattering. *Spectrochim. Acta Part A Mol. Biomol. Spectrosc.* **2008**, *69*, 91–95. [CrossRef] [PubMed]